TOWARDS A FULLY INTEGRATED AND DISPOSABLE DNA AMPLIFICATION CHIP

*F. Akegawa Monteiro[1], H.-W. Veltkamp[1 *], R.G.P. Sanders[1], R.J. Wiegerink[1], and J.C. Lötters[1,2]*
[1] MESA+ Institute for Nanotechnology, University of Twente, Enschede, The Netherlands
[2] Bronkhorst High-Tech BV, Ruurlo, The Netherlands

ABSTRACT

Fast point-of-use detection of early-stage zoonoses is beneficial for animal husbandry as it can save livestock and prevent farmers from going bankrupt after an outbreak. This paper describes the first steps towards a fully integrated and disposable DNA amplification chip. Based on the analysis of the milling process, metal adhesion study, COMSOL Multiphysics heat transfer simulations and chip characterization a feasible fabrication process is set up and the first batch of chips has been fabricated.

KEYWORDS

Zoonoses detection, on-chip DNA amplification, integrated heaters, disposable chips

INTRODUCTION

Zoonoses is a widespread problem in animal husbandry[1]. This group encompasses diseases which can be transferred between animals (usually vertebrates) and humans. They are transmitted through zoonotic agents (e.g. bacteria, virus, fungi, and parasites)[2]. An infamous example would be *Coxiella burnetii* (Q-fever)[2]. These diseases are of potential risk for livestock of farms. An outbreak among the livestock is disastrous to the owner of that farm, and for people living in the proximity of that farm[3]. Often, more animals of the livestock are infected and the whole livestock is exterminated out of precaution, which could lead to bankruptcy of the farmer. Therefore, early-stage detection is often the key to save livestock and farms. As these diseases are also encountered in developing countries, where farms are often remotely located, it is desired that such detection equipment is portable and as cheap as possible. A lab-on-a-chip platform can be used for this early-stage detection.

In the early stage of these diseases, the agent, and therefore its DNA, are not widespread in the infected animal, making the detection rather difficult. A detection system has to amplify the DNA of the disease until a certain threshold is reached and detection is possible. When this amplification reaction is sequence specific, for example by using polymerase chain reaction (PCR) or helicase-dependent amplification (HDA), and when a fluorescent DNA dye is used, a simple yes-or-no answer for a specific disease can be obtained. In the past, several chip-based DNA amplification devices with fluorescence detection were reported. However, in these devices heat supply for the DNA amplification reaction often comes from an external heat source[4] or is processed in a different substrate and later incorporated onto the chip[5]. A challenge that seems to remain is to incorporate heaters on a disposable, often polymeric, substrate. Incorporation of heaters will simplify the required equipment and therefore, lower its costs.

The work presented here aims at the development of a disposable, polymeric DNA amplification lab-on-chip system with integrated resistive heaters and fluorescence detection. The choice of substrate material, deposition method, and metal are studied. Although, it is mentioned above that PCR and HDA are sequence specific, the model reaction chosen is multiple displacement amplification (MDA). This reaction is more straightforward, as it amplifies any present double stranded DNA, and is therefore better suitable as a proof-of-principle amplification reaction to show the functioning of the integrated heaters.

CHIP DESIGN

A chamber-based amplification chip is designed based on the work of Bruijns *et al.*[5]. Using SolidWorks 2018 CAD/CAE software, the 3D image of the chip is drawn and with the AutoDesk HSMWorks CAD/CAM plug-in, this image is transferred into computer numerical control (CNC) milling code. The total chip size is $3\,\mathrm{cm}$ by $3\,\mathrm{cm}$ and has a chamber of $10\,\mathrm{mm}$ by $3\,\mathrm{mm}$. Two trapezoid structures are placed in the tapered channels between the inlet/outlet and the chamber. The function of these trapezoids is twofold. Firstly, they minimize the dead volume between the inlet/outlet and the reaction chamber, locating as much as possible of the reaction mixture inside the chamber. Secondly, they provide support for the chamber closure. A rectangular channel is located next to the reaction chamber and is also covered by the heaters. A thermocouple is inserted in this channel for

real-time monitoring of the temperature inside the chip. In figure 1 the SolidWorks design of the chamber-based chip is shown.

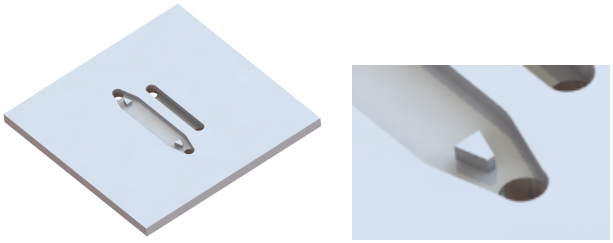

Figure 1: SolidWorks drawing of the DNA amplification chamber. This drawing is used to set up the code for the CNC mill. The small rectangular channel next to the chamber is for thermocouple-assisted real-time temperature monitoring. Total size of the chip is 3 cm by 3 cm. The close-up shows the in-channel trapezoid structure.

The heater structure will be placed at the bottom side of the chip using shadow masks. To determine the optimal heater width and heater spacing, a parametric study using COMSOL Multiphysics 5.3a finite element method simulations with the *Heat Transfer in Solids* (ht) package is done. The model is designed such that it consists of two parallel rectangles of COC (in the real device, the upper plate is a PCR adhesive foil) with water in between. The heaters are assumed to be lines. This reduces the required quality of the mesh tremendous, as the heaters in the real device will be around $100\,\mathrm{nm}$.

In figure 2, the results of two different heater widths and heater spacings are shown. The heater width for both geometries is $0.3\,\mathrm{mm}$, while the heater spacing in the left and right image are $0.3\,\mathrm{mm}$ and $2.0\,\mathrm{mm}$, respectively. In figure 3a and 3b, tables with the temperature deviation between the highest and lowest temperature at the top of the chamber ($\Delta T_{\text{top of channel}} = T_{top,max} - T_{top,min}$) and the deviation between the set heater temperature of $30\,^{\circ}\mathrm{C}$ and the lowest temperature at the top of the chamber ($\Delta T_{\text{deviation from set T}} = T_{heater} - T_{top,min}$) are shown for different heater widths and heater spacings. Based on these results, a meandering heater pattern of a $0.3\,\mathrm{mm}$ wide heater with $0.3\,\mathrm{mm}$ spacing in between the lines is designed. The pattern is divided over two shadow masks to prevent curvature of the long stainless steel beams in between the meandering structure.

FABRICATION

Cyclic olefin copolymer (COC)[6] is chosen as polymeric substrate due to its bio-compatibility, optical transparency, physical resistance, electrical insulation, and price. Injection molded COC plates of $10\,\mathrm{cm}$ by $10\,\mathrm{cm}$ and $1.5\,\mathrm{mm}$ thickness of the grade TOPAS 6017 are obtained via Kunststoff-Zentrum Leipzig. This grade is chosen because of its relatively high glass transition temperature ($\mathrm{T_g} = 170\,^{\circ}\mathrm{C}$), which minimizes melting during the milling process. The microfluidic structure explained in section is CNC-milled using a Mikron WF 21C milling machine. The milling causes a considerable loss of optical transparency due to the created roughness. This could obstruct the fluorescence detection. Therefore, a chemical post-treatment with cyclohexane vapor is done, such treatment dissolves the upper layer of COC and causes reflowing of the material due to its surface tension, restoring the optical transparency and reducing the surface roughness[7].

Metal is deposited on the substrate using laser-cut Mo shadow masks to outline the shape of the resistive heaters. Mo has a smaller coefficient of thermal expansion and is therefore chosen instead of stainless steel. Metals of interest are Au or Pt, which are commonly used metals to function as resistive heaters[8]. The deposition methods studied are DC magnetron sputtering and e-beam physical vapor deposition (evaporation). Both methods are capable of large-scale production, which will lower the production costs on an industrial scale. The metal and deposition method will be chosen based on the metal adhesion performances on the COC substrate, which is studied using the Scotch tape test[9], and the resistance versus temperature behavior in the range $20\,^{\circ}\mathrm{C}$ – $100\,^{\circ}\mathrm{C}$, which is measured in a customized Heraeus T5025 oven with electrical readout.

The chambers with the resistive heaters on the backside are closed using Microseal 'B' PCR plate sealing film from Bio-Rad, which is cut in the proper size and manually attached on top of the substrate. The reaction mixture containing DNA and the amplification mixture is pipetted inside the chip using the inlet aperture, and the inlet and outlet are closed using the same PCR film. A power is applied on the resistive heaters until they acquire the desired temperature for the amplification. The initial power is based on the resistance measurements, but will be adjusted according to the feedback loop of the thermocouple. Detection of the amplification is done by using an Horiba Scientific FluoroMax+ spectrofluorometer, but will in the near future be done by *in-situ* fluorescence measurements using an optical fiber together with the FluoroMax+.

RESULTS

The process towards a fully integrated and

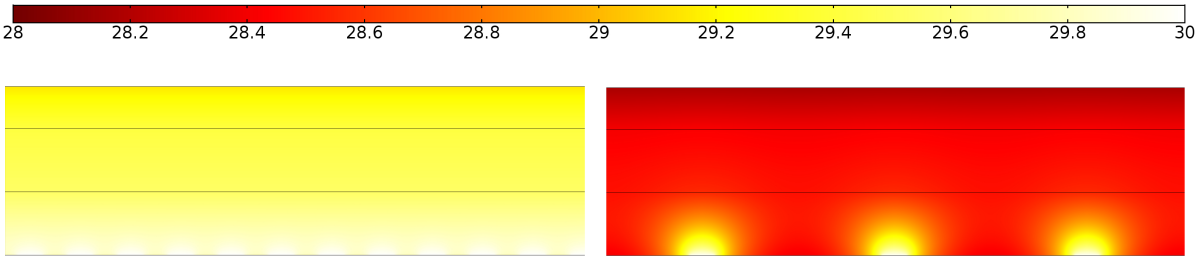

(a) 0.3 mm width and 0.3 mm spacing. *(b) 0.3 mm width and 2.0 mm spacing.*

Figure 2: COMSOL heat transfer simulations of a 0.75 mm deep chamber with different heater widths and heater spacings. The scale bar applies to figure 2a and 2b.

	0.3	0.4	0.5	0.6	0.7	0.8	0.9	1.0	1.1	1.2	1.3	1.4	1.5	1.6	1.7	1.8	1.9	2.0
0.3	0.000	0.001	0.001	0.001	0.001	0.002	0.001	0.001	0.001	0.001	0.001	0.001	0.001	0.003	0.001	0.003	0.004	0.002
0.4	0.001	0.001	0.002	0.001	0.002	0.001	0.002	0.001	0.001	0.001	0.001	0.002	0.002	0.001	0.003	0.004	0.003	0.002
0.5	0.001	0.002	0.001	0.003	0.001	0.002	0.001	0.001	0.001	0.002	0.002	0.002	0.003	0.006	0.003	0.003	0.003	0.006
0.6	0.003	0.001	0.003	0.002	0.002	0.002	0.004	0.001	0.002	0.002	0.004	0.002	0.004	0.006	0.004	0.004	0.007	0.005
0.7	0.002	0.004	0.002	0.003	0.002	0.002	0.006	0.002	0.003	0.003	0.003	0.006	0.007	0.006	0.005	0.009	0.007	0.009
0.8	0.005	0.002	0.003	0.002	0.002	0.002	0.002	0.005	0.005	0.003	0.006	0.007	0.007	0.007	0.011	0.008	0.012	0.011
0.9	0.003	0.004	0.003	0.007	0.008	0.003	0.005	0.006	0.004	0.008	0.009	0.008	0.008	0.012	0.010	0.014	0.013	0.013
1.0	0.006	0.004	0.003	0.004	0.004	0.006	0.006	0.006	0.009	0.010	0.010	0.010	0.015	0.012	0.017	0.017	0.017	0.017
1.1	0.005	0.003	0.004	0.004	0.007	0.008	0.006	0.010	0.012	0.011	0.011	0.018	0.014	0.019	0.019	0.019	0.020	0.030
1.2	0.005	0.005	0.005	0.008	0.008	0.007	0.011	0.013	0.013	0.013	0.020	0.016	0.022	0.021	0.022	0.024	0.034	0.030
1.3	0.006	0.006	0.009	0.010	0.008	0.014	0.015	0.015	0.015	0.022	0.018	0.024	0.025	0.026	0.027	0.038	0.034	0.033
1.4	0.008	0.012	0.012	0.009	0.015	0.018	0.016	0.017	0.025	0.020	0.027	0.027	0.029	0.030	0.043	0.038	0.037	0.040
1.5	0.014	0.013	0.011	0.017	0.020	0.018	0.018	0.028	0.022	0.030	0.030	0.032	0.049	0.048	0.042	0.042	0.044	0.053
1.6	0.017	0.012	0.020	0.023	0.020	0.019	0.031	0.024	0.034	0.034	0.035	0.037	0.053	0.047	0.046	0.048	0.058	0.060
1.7	0.014	0.023	0.027	0.022	0.021	0.034	0.026	0.036	0.037	0.039	0.040	0.058	0.051	0.049	0.053	0.064	0.065	0.067
1.8	0.027	0.033	0.024	0.023	0.038	0.028	0.04	0.040	0.041	0.043	0.062	0.056	0.054	0.057	0.069	0.072	0.074	0.077
1.9	0.039	0.027	0.025	0.041	0.030	0.043	0.043	0.044	0.047	0.068	0.061	0.059	0.062	0.076	0.077	0.080	0.083	0.086
2.0	0.031	0.026	0.046	0.032	0.047	0.047	0.048	0.049	0.074	0.065	0.062	0.066	0.082	0.083	0.086	0.090	0.093	0.096

(a) $\Delta T_{top\ of\ channel} = T_{top,max} - T_{top,min}$.

	0.3	0.4	0.5	0.6	0.7	0.8	0.9	1.0	1.1	1.2	1.3	1.4	1.5	1.6	1.7	1.8	1.9	2.0
0.3	0.585	0.574	0.566	0.560	0.555	0.552	0.548	0.546	0.544	0.542	0.540	0.539	0.538	0.538	0.535	0.536	0.537	0.534
0.4	0.626	0.608	0.597	0.587	0.581	0.574	0.570	0.565	0.562	0.559	0.556	0.555	0.553	0.550	0.550	0.550	0.547	0.545
0.5	0.671	0.649	0.631	0.620	0.609	0.601	0.594	0.588	0.583	0.579	0.576	0.573	0.570	0.568	0.568	0.563	0.561	0.562
0.6	0.722	0.691	0.672	0.654	0.642	0.631	0.624	0.614	0.608	0.603	0.599	0.593	0.591	0.589	0.584	0.581	0.581	0.576
0.7	0.774	0.740	0.712	0.693	0.676	0.663	0.656	0.643	0.636	0.629	0.622	0.619	0.615	0.609	0.604	0.604	0.598	0.597
0.8	0.832	0.787	0.757	0.733	0.714	0.698	0.685	0.676	0.666	0.656	0.651	0.645	0.638	0.632	0.631	0.623	0.622	0.617
0.9	0.888	0.840	0.804	0.780	0.759	0.736	0.722	0.709	0.696	0.689	0.681	0.671	0.664	0.661	0.652	0.650	0.644	0.639
1.0	0.950	0.893	0.852	0.821	0.796	0.777	0.759	0.743	0.732	0.721	0.710	0.700	0.696	0.685	0.682	0.675	0.669	0.663
1.1	1.010	0.947	0.902	0.867	0.841	0.818	0.796	0.782	0.768	0.753	0.741	0.736	0.722	0.717	0.709	0.701	0.694	0.697
1.2	1.072	1.004	0.954	0.918	0.886	0.858	0.839	0.821	0.803	0.787	0.780	0.763	0.757	0.746	0.737	0.729	0.731	0.719
1.3	1.136	1.062	1.010	0.967	0.930	0.906	0.882	0.859	0.839	0.829	0.809	0.801	0.788	0.777	0.767	0.768	0.754	0.744
1.4	1.201	1.125	1.065	1.015	0.982	0.952	0.922	0.898	0.885	0.860	0.850	0.834	0.821	0.809	0.809	0.793	0.781	0.774
1.5	1.271	1.184	1.117	1.072	1.033	0.995	0.964	0.947	0.917	0.904	0.885	0.869	0.870	0.854	0.835	0.822	0.812	0.810
1.6	1.338	1.241	1.179	1.127	1.078	1.039	1.018	0.981	0.965	0.942	0.922	0.905	0.903	0.881	0.865	0.854	0.851	0.841
1.7	1.399	1.310	1.240	1.175	1.126	1.097	1.053	1.032	1.005	0.981	0.960	0.957	0.931	0.912	0.899	0.896	0.883	0.872
1.8	1.476	1.378	1.290	1.226	1.189	1.134	1.108	1.074	1.045	1.020	1.015	0.986	0.964	0.948	0.943	0.929	0.916	0.905
1.9	1.552	1.430	1.344	1.294	1.227	1.193	1.152	1.117	1.087	1.080	1.046	1.020	1.001	0.995	0.978	0.963	0.950	0.938
2.0	1.607	1.487	1.419	1.334	1.290	1.240	1.197	1.160	1.151	1.111	1.080	1.059	1.051	1.031	1.014	0.999	0.985	0.972

(b) $\Delta T_{deviation\ from\ set\ T} = T_{heater} - T_{top,min}$.

Figure 3: Temperature differences for different heater widths (0.3 mm to 2.0 mm, in the columns) and heater spacings (0.3 mm to 2.0 mm, in the rows), obtained using a parametric sweep in the COMSOL Multiphysics heat transfer simulations.

disposable DNA amplification chip can be divided into several smaller steps, each with their own results. These steps are discussed in the following subsections.

Optical transparency

With the reported surface treatment[7] we were capable of increasing the optical transmittance fivefold. Cyclohexane vapor treatment duration is depending on the grade of COC and the initial surface roughness, which on its turn is depending on the milling machine, dept, speed, etc. The transmittance measurements are done using a Woollam M-2000UI ellipsometer. The surface roughness, measured using a Bruker Icon Dimension atomic force microscope and Gwyddion 2.52 software, decreased from $310.10\,\mathrm{nm}$ to $0.97\,\mathrm{nm}$ (compared to $3.50\,\mathrm{nm}$ for pristine COC).

Metal adhesion

In order to get the most reliable heaters, four possible options are investigated. The adhesion of Au and Pt deposited by either PVD or e-beam sputtering is investigated using the Scotch tape test[9]. Test patterns consisting of rectangular strips of $2\,\mathrm{mm}$ by $14\,\mathrm{mm}$ are fabricated by depositing $100\,\mathrm{nm}$ of metal using a shadow mask made out of Kapton foil. Based on the results in table 1, the choice of heater material is sputtered Au.

Table 1: Results of the Scotch tape metal adhesion tests before and after heat cycling. Here, + means passing the tape test, − means failing the tape test, and +/− means that not all test structures failed the tape test.

Material	Method	Tape test		Initial
		Before	After	resistance [Ω]
Au	PVD	+	−	5.0
Au	Sputtering	+	+	8.2
Pt	PVD	+	+	400
Pt	Sputtering	+	+/−	6.8

Chip functioning

Characterization of the actual heater is done using a FLIR One Pro iOS thermal camera. Thermal images of the heater structure are made while different input powers are used to heat up the heaters. The images are processed using ImageJ post-processing software. Results of these measurements are shown in figure 4.

The reliability of the heaters is tested by inserting a 162 series RS Technics thermocouple K into the reference channel. A constant input potential of $4\,\mathrm{V}$ is applied and the temperature is measured for $24\,\mathrm{h}$. This exceeds the required operation time at least twelve-fold, meaning that it is a good indication for the reliability of the heater. The results are shown in figure 5.

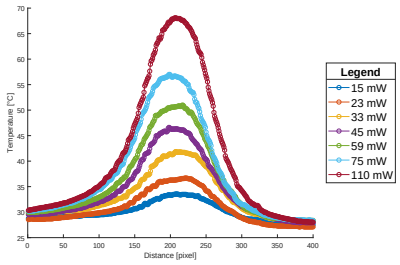

Figure 4: Temperature profiles over the heater structure for different input powers. Measurements are done using a FLIR One Pro iOS thermal camera.

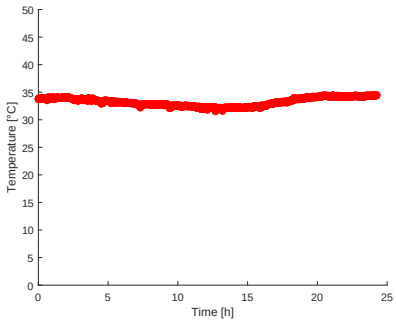

Figure 5: Duration test of the heater. A constant potential of 4 V is applied and the temperature is measured for 24 h.

DNA amplification

In figure 6, graphs of the fluorescence signal during MDA reactions at 25 °C and 30 °C, together with their non template control (NTC) are shown. These reactions are carried out in a conventional PCR machine and the results show that the chosen proof-of-principle DNA amplification reaction is temperature dependent to some extend, but that there is a wide range of temperatures at which the amplification can be performed. This makes the functioning of the integrated resistive heaters less critical.

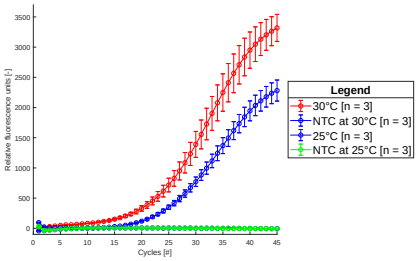

Figure 6: Fluorescence signal of MDA reactions performed at 25°C and 30°C, together with their (overlapping) NTCs.

CONCLUSION

With the obtained results of the steps towards a fully integrated and disposable DNA amplification chip, the conclusion can be made the realization of such a system will be achieved within a month after the Microfluidic Handling Systems Conference. The CNC milling and subsequent cyclohexane vapor treatment for regaining the optical transparency, and the use of adhesive PCR plate sealing film give well-defined reaction chambers. The sputtering of Au gives heater structures with good adhesion properties on COC and a long-term stability exceeding the required operation time by many hours (stability over 24 h is ±1.5 °C). All fabrication methods are chosen in such way that the production of the devices could easily be scaled-up to large-scale manufacturing plants.

ACKNOWLEDGMENTS

The authors would like to thank dr. Brigitte Bruijns from Micronit Microtechnologies for her help during the brainstorm sessions. Jörg Strack from TOPAS Advanced Polymers and dr. Thomas Wagenknecht from KUZ Leipzig are thanked for their information on COC. Pieter Post, Rob Dierink and Sip Jan Boorsma of TCO (technical center for education and research of the University of Twente) are thanked for their work in the milling and laser cutting processes, dr. Christian Bruinink for his assistance in the transparency measurements, Daniel Monteiro Cunha, M.Sc. for his assistance in the AFM measurements, and Nikki Stroot for her assistance with the initial amplification reactions.

REFERENCES

[1] B. Shin *et al. Front. Vet. Sci.*, 5(1):166/1–9, 2018. doi: 10.3389/fvets.2018.00166.

[2] L. Cantas *et al. Front. Public Health*, 2(144):1–8, 2014. doi: 10.3389/fpubh.2014.00144.

[3] W. van der Hoek *et al. Adv. Exp. Med. Biol.*, 984:329–364, 2012. doi: 10.1007/978-94-007-4315-1_17.

[4] W. Wu *et al. Anal. Bioanal. Chem.*, 400(7):2053–2060, 2011. doi: 10.1007/s00216-011-4947-x.

[5] B. B. Bruijns *et al. Sensor. Actuat. B-Chem.*, 293(1):16–22, 2019. doi: 10.1016/j.snb.2019.04.144.

[6] Topas Advanced Polymers. URL `https://topas.com/sites/default/files/files/TOPAS_Brochure_E_2014_06(1).pdf`. [Last accessed: Jun. 18, 2019].

[7] I. R. G. Ogilvie *et al. J. Micromech. Microeng.*, 20(6):065016/1–8, 2010. doi: 10.1088/0960-1317/20/6/065016.

[8] V. Miralles *et al. Diagnostics*, 3(1):33–67, 2013. doi: 10.3390/diagnostics3010033.

[9] I. F. Silvera *et al. Rev. Sci. Instrum.*, 57(7):1381–1383, 1986. doi: 10.1063/1.1138605.

CONTACT

Henk-Willem Veltkamp, h.veltkamp@utwente.nl